The hydrogen–air burning rate near the lean flammability limit

D. Fernández-Galisteo,[a] A.L. Sánchez,[a*] A. Liñán[b] and F.A. Williams[c]

Dept. Ingeniería Térmica y de Fluidos, Universidad Carlos III de Madrid, Madrid, Spain; [b]ETSI Aeronáuticos, Universidad Politécnica de Madrid, Madrid, Spain; [c]Dept. of Mechanical and Aerospace Engineering, University of California San Diego, CA, USA

This paper investigates the inner structure of the thin reactive layer of hydrogen–air fuel-lean deflagrations close to the flammability limit. The analysis, which employs seven elementary reactions for the chemistry description, uses the ratio of the characteristic radical and fuel concentrations as a small asymptotic parameter, enabling an accurate analytic expression for the resulting burning rate to be derived. The analysis reveals that the steady-state assumption for chemical intermediaries, applicable on the hot side of the reactive layer, fails, however, as the crossover temperature is approached, providing a nonnegligible higher-order correction to the burning rate. The results can be useful, for instance, in future investigations of hydrogen deflagration instabilities near the lean flammability limit.

Keywords: burning rate; hydrogen; laminar flame; asymptotic theory; lean combustion

1. Introduction

Theoretical investigations of flame dynamics often take into account that the structure of planar steady deflagrations typically involves two layers, a frozen upstream preheat region and a much thinner diffusive-reactive layer with negligible effects of convection. In the presence of flame perturbations, unsteady effects, as well as curvature and strain effects, enter first to modify the thicker preheat region, while the reactive-diffusive layer behaves as planar in the first approximation and reacts to the external perturbations in a quasi-steady manner, giving a burning rate (fuel burnt per unit flame surface per unit time) that is mainly a function of the perturbed burnt temperature. This paper is intended to facilitate perturbation analyses by providing a simplified description for the resulting burning rate for hydrogen–air flames near the lean flammability limit, to be used, for instance, in the investigation of diffusive-thermal instabilities leading to cellular structures in such flames and in the study of the dynamics of these flames under perturbations.

The present work builds on our previous investigation [1], which identified a detailed mechanism of seven elementary reactions, shown below in Table 1, that describes accurately the propagation of atmospheric and sub-atmospheric lean hydrogen–air flames. The resulting chemistry description predicts, in particular, a kinetically controlled flammability limit at which the planar deflagration velocity vanishes, when the adiabatic flame temperature equals the crossover temperature, T_c, the latter defined such that the rate of reaction $H + O_2$

Table 1. The seven-step mechanism with rate coefficients in the Arrhenius form $k = AT^n \exp(-T_a/T)$ as given in [3].

Reaction		A[a]	n	T_a[K]
1. $H+O_2 \rightleftharpoons OH+O$[b]	k_f	3.52×10^{16}	-0.7	8590
	k_b	7.04×10^{13}	-0.264	72
2. $H_2+O \rightleftharpoons OH+H$[b]	k_f	5.06×10^{4}	2.67	3166
	k_b	3.03×10^{4}	2.633	2433
3. $H_2+OH \rightleftharpoons H_2O+H$[b]	k_f	1.17×10^{9}	1.3	1829
	k_b	1.29×10^{10}	1.196	9412
4f. $H+O_2+M \rightarrow HO_2+M$[c]	k_0	5.75×10^{19}	-1.4	0
	k_∞	4.65×10^{12}	0.44	0
5f. $HO_2+H \rightarrow OH+OH$		7.08×10^{13}	0	148
6f. $HO_2+H \rightarrow H_2+O_2$		1.66×10^{13}	0	414
7f. $HO_2+OH \rightarrow H_2O+O_2$		2.89×10^{13}	0	-250

[a]Units are mol, s, cm^3, and K.
[b]The backward rate parameters are approximate fits obtained from the forward rate parameters by use of the thermodynamic data.
[c]Chaperon efficiencies are 2.5 for H_2, 16.0 for H_2O, and 1.0 for all other species; Troe falloff with $F_c = 0.5$ [5].

$\overset{1f}{\rightarrow}$ OH+O equals that of reaction $H + O_2 + M \overset{4f}{\rightarrow} HO_2 + M$. It is found that for the temperature conditions typically encountered the reaction constants are such that the concentrations of O, OH and HO_2 are much smaller than that of H_2 and consequently can be treated in the steady-state approximation at leading order. On the other hand, the ratio of the H and H_2 concentrations in the reaction layer will be found to be of the order of the ratio of the H_2 and O_2 concentrations there, and therefore is proportional to $(T_b - T_c)/(T_b - T_u)$, with T_u and T_b representing the initial temperature of the unburnt mixture and the burnt temperature, respectively. When, for lean flames close to the flammability limit, the burnt temperature T_b is close to the crossover value T_c, the resulting H-atom concentration is much smaller than the H_2 concentration in the reaction layer, thereby ensuring the applicability of the steady-state approximation at leading order also for H atoms. With all radicals maintaining chemical-kinetic steady states in the first approximation, the development leads to a one-step reduced mechanism in which the main species react according to the single overall reaction $2H_2 + O_2 \rightarrow 2H_2O$ with a non-Arrhenius global rate. The resulting steady-state expressions for H, O and OH predict radicals to exist only in a small intermediate temperature range that extends from crossover to the burnt temperature T_b. Radicals disappear abruptly at crossover where the resulting radical profiles exhibit an unrealistic discontinuous slope and the steady-state assumptions fail.

The analysis below will use the ratio, ε, of the characteristic values of the H-atom and H_2 concentrations in the reaction layer as a small asymptotic parameter for the description of the reaction zone in lean hydrogen–air deflagrations. For the temperatures typically encountered, this small parameter satisfies $\varepsilon \sim (T_b - T_c)/(T_b - T_u)$, and therefore is also proportional to the ratio of the reaction-layer thickness to the flame thickness. Small values of ε, associated with values of the burnt temperature T_b close to T_c, therefore also imply that convection can be neglected in the first approximation in the reaction zone. The analysis of the resulting diffusive-reactive layer, including the region where steady-state approximations hold for all radicals and the layer of steady-state failure, located around the crossover temperature, will provide, in particular, the burning rate as a function of the

burnt temperature and the pressure, which will be tested by comparisons of predictions of propagation velocities of steady planar flames, employing the seven-step mechanism along with our previous [1] assumptions concerning transport, in order to be able to evaluate better how accurate the results of the present development may be.

2. Specific objectives and problem formulation

As shown recently [1], for hydrogen–air mixtures that are very fuel lean, the seven steps shown in Table 1 suffice to describe accurately flame propagation velocity. The table shows the rate constants for all reactions, taken from the so-called San Diego mechanism [2], which has been tested to give excellent results when applied to the description of hydrogen combustion [3].

A sample computation of a steady planar deflagration obtained with the COSILAB code [4] with this seven-step mechanism is shown in Figure 1 for pressure $p = 1$ atm, initial temperature $T_u = 300$ K and equivalence ratio $\phi = 0.28$. As can be seen, for these very lean conditions radicals only exist in a relatively thin reactive layer that is preceded by a chemically frozen preheat region. The main effect of curvature and unsteadiness, together with preferential diffusion effects, is to change the structure of the preheat region from that shown in the figure for a steady planar flame, modifying the burnt temperature and, therefore, the resulting burning rate.

We shall investigate below the structure of the thin reactive layer where radicals are present to determine the fuel mass burning rate as a function of the burnt temperature, giving results that may be used not only for computations of steady planar deflagration velocities but also in studies of flame dynamics and stability. Because of its small thickness, convection can be neglected in the first approximation in this reactive layer, along with changes of density ρ and thermal diffusivity D_T from their downstream values at equilibrium. If n is defined as the coordinate normal to the reaction layer, then the resulting species conservation

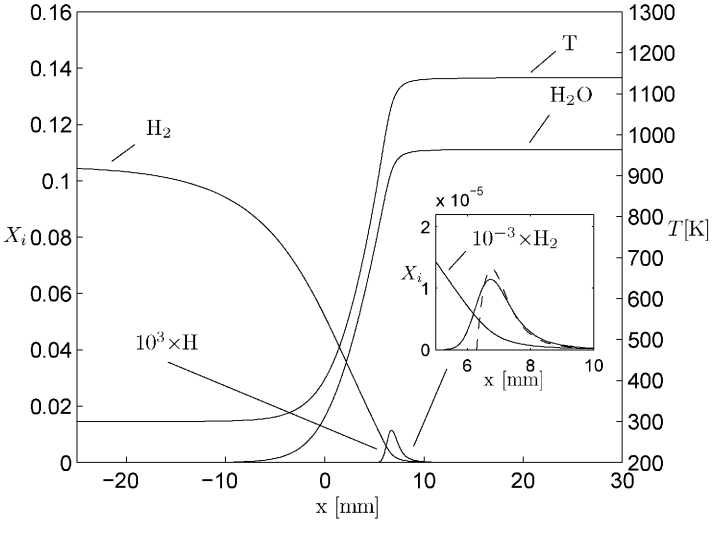

Figure 1. The temperature and mole fractions across a premixed hydrogen–air mixture for $p = 1$ atm, $T_u = 300$ K and $\phi = 0.28$ as calculated with the seven-step short mechanism; the inset compares the H-atom mole fraction computed numerically with that predicted by the steady-state expression (29).

equations become

$$-\frac{D_T}{L_{H_2}}\frac{d^2C_{H_2}}{dn^2} = \dot{C}_{H_2} = -\omega_2 - \omega_3 + \omega_{6f} \tag{1}$$

$$-\frac{D_T}{L_{O_2}}\frac{d^2C_{O_2}}{dn^2} = \dot{C}_{O_2} = -\omega_1 - \omega_{4f} + \omega_{6f} + \omega_{7f} \tag{2}$$

$$-\frac{D_T}{L_{H_2O}}\frac{d^2C_{H_2O}}{dn^2} = \dot{C}_{H_2O} = \omega_3 + \omega_{7f} \tag{3}$$

$$-\frac{D_T}{L_O}\frac{d^2C_O}{dn^2} = \dot{C}_O = \omega_1 - \omega_2 \tag{4}$$

$$-\frac{D_T}{L_{OH}}\frac{d^2C_{OH}}{dn^2} = \dot{C}_{OH} = \omega_1 + \omega_2 - \omega_3 + 2\omega_{5f} - \omega_{7f} \tag{5}$$

$$-\frac{D_T}{L_H}\frac{d^2C_H}{dn^2} = \dot{C}_H = -\omega_1 + \omega_2 + \omega_3 - \omega_{4f} - \omega_{5f} - \omega_{6f} \tag{6}$$

$$-\frac{D_T}{L_{HO_2}}\frac{d^2C_{HO_2}}{dn^2} = \dot{C}_{HO_2} = \omega_{4f} - \omega_{5f} - \omega_{6f} - \omega_{7f} \tag{7}$$

where C_i and L_i are the concentration and Lewis number of species i, and $\dot{C}_i$ denotes its corresponding chemical production rate (moles per unit volume per unit time), to be computed from the rates ω_j of the elementary reactions shown in Table 1. At the same level of approximation, the energy conservation equation becomes

$$\rho c_p D_T \frac{d^2T}{dn^2} = \sum h_i^o \dot{C}_i, \tag{8}$$

where c_p is the specific heat at constant pressure, assumed to be constant, T is the temperature, and h_i^o is the enthalpy of formation per mol of species i at T_b. The above equations are to be integrated with boundary conditions corresponding to matching with the upstream chemically frozen preheat region as $n \to -\infty$

$$\frac{\dot{m}_{H_2}}{W_{H_2}D_T} = -\frac{1}{L_{H_2}}\frac{dC_{H_2}}{dn} = -\frac{2}{L_{O_2}}\frac{dC_{O_2}}{dn} = \frac{1}{L_{H_2O}}\frac{dC_{H_2O}}{dn} = -\frac{\rho c_p}{h^o_{H_2O}}\frac{dT}{dn} \tag{9}$$

and

$$C_O = C_{OH} = C_H = C_{HO_2} = 0, \tag{10}$$

where $\dot{m}_{H_2}$ is the mass fuel burning rate and W_{H_2} is the molecular mass of H_2. The accompanying boundary conditions as $n \to +\infty$ correspond to the downstream state reached as the gradients of concentrations and temperature vanish

$$C_{H_2} = C_{O_2} - C_{O_{2b}} = C_{H_2O} - C_{H_2O_b} = C_O = C_{OH} = C_H = C_{HO_2} = T - T_b = 0, \tag{11}$$

where the subscript b denotes conditions in the burnt gas.

Note that in a planar steady deflagration, the burnt conditions can be computed as the chemical equilibrium state for the fresh gas mixture upstream from the preheat region, so that in particular the burnt temperature T_b would be equal to the adiabatic flame temperature T_∞. In the presence of flame perturbations, however, unsteady effects, as well as curvature and strain effects, enter to modify the flame structure in the thick preheat region that precedes the reaction zone, causing the value of T_b to differ from the adiabatic flame temperature. In particular, lean hydrogen flames are known to be strongly prone to diffusive-thermal instabilities that induce departures from presumed steady, planar structures. In the resulting curved flames, because of differential diffusion effects the burnt temperature T_b is larger than the adiabatic flame temperature T_∞ in the convex parts of the flame, and smaller in the concave parts. When the departures are sufficiently small for T_b to remain above the crossover value everywhere, hydrogen is depleted behind the reaction sheet, which is followed by a postflame region in chemical equilibrium, of thickness comparable to or larger than that of the preheat region. Across this region transverse heat conduction causes the solution to evolve slowly from the burnt state with $T = T_b$ found immediately downstream from the reaction zone towards the final equilibrium state with $T = T_\infty$. When the flame perturbations are such that $T_\infty - T_b \ll T_\infty$ the gradients found in this postflame region are much smaller than those found in the reaction zone and can be therefore neglected in the first approximation when computing the burning rate, which can be determined with consideration of vanishing gradients downstream from the reaction zone, a condition employed above when writing the boundary conditions (11).

On the other hand, for conditions near the lean flammability limit, relatively small temperature excursions $T_\infty - T_b$ in curved flames may lead to values of the burnt temperature below crossover in the concave parts of the flame, leading to local extinction of the chemical reaction and to the appearance of cellular flames, seen in recent numerical simulations [6]. These cellular flames, which could be investigated with the one-step chemistry recently derived [1], exist even for equivalence ratios well below the kinetically controlled flammability limit of planar flames. Because of their relatively large curvature, peak temperatures above crossover are found behind the reaction layer in each individual flame cell, whose hot products mix downstream with the cold reactant mixture that flows between cells, leading to a relatively cold postflame region where chemical reaction proceeds at a negligibly slow rate. These cellular flames fall outside the scope of the present analysis, which considers weakly perturbed flames with burned temperatures above crossover such that the downstream zone does not influence the preheat or reaction zones, its properties departing negligibly from those of the equilibrium state.

The solution of the above problem for given values of T_b, $C_{O_2 b}$, $C_{H_2O_b}$ and pressure determines the fuel burning rate $\dot{m}_{H_2}$. To facilitate the development, it is convenient to combine linearly (1), (2) and (3) with (4)–(7) to obtain the alternative equations

$$D_T \frac{d^2}{dn^2}\left(\frac{C_{H_2}}{L_{H_2}} + \frac{C_O}{L_O} + \frac{1}{2}\frac{C_{OH}}{L_{OH}} + \frac{3}{2}\frac{C_H}{L_H} - \frac{1}{2}\frac{C_{HO_2}}{L_{HO_2}}\right) = 2\omega_{4f} \tag{12}$$

$$D_T \frac{d^2}{dn^2}\left(\frac{C_{O_2}}{L_{O_2}} + \frac{C_O}{L_O} + \frac{1}{2}\frac{C_{OH}}{L_{OH}} + \frac{1}{2}\frac{C_H}{L_H} + \frac{1}{2}\frac{C_{HO_2}}{L_{HO_2}}\right) = \omega_{4f} \tag{13}$$

$$D_T \frac{d^2}{dn^2}\left(\frac{C_{H_2O}}{L_{H_2O}} - \frac{C_O}{L_O} - \frac{C_H}{L_H} + \frac{C_{HO_2}}{L_{HO_2}}\right) = -2\omega_{4f}, \tag{14}$$

where

$$\omega_{4f} = k_{4f} C_{\mathrm{M}} C_{\mathrm{O}_2} C_{\mathrm{H}} \tag{15}$$

is the rate of the three-body recombination reaction, with

$$C_{\mathrm{M}} = p/(R^o T) + 15 C_{\mathrm{H_2O}} + 1.5 C_{\mathrm{H}_2} \tag{16}$$

representing the effective third-body concentration, which accounts for the non-unity third-body chaperon efficiencies of water vapor and molecular hydrogen. Integrating once (12) with the boundary conditions given above provides

$$\dot{m}_{\mathrm{H}_2} = 2 W_{\mathrm{H}_2} \int_{-\infty}^{+\infty} k_{4f} C_{\mathrm{M}} C_{\mathrm{O}_2} C_{\mathrm{H}} \mathrm{d}n, \tag{17}$$

indicating that the burning rate is linearly proportional to rate of the recombination reaction $4f$ integrated across the flame. An accurate description of the H-atom concentration is therefore needed to compute $\dot{m}_{\mathrm{H}_2}$. We shall see below that such a description requires consideration of two different regions: a relatively thick layer where all radicals follow a steady-state approximation to leading order and a thinner upstream layer where the steady-state approximations for O, OH and H break down. Both regions will be analyzed separately below and their corresponding contributions to the burning rate will be determined.

3. Fuel burning rate based on analysis of the steady-state region

As seen in Figure 1 for the radical H, taken as representative of the radical pool, near the lean flammability limit radicals appear in concentrations that are much smaller than those of H_2. Neglecting radical concentrations on the left-hand side of (12), (13) and (14) provides

$$\frac{D_T}{L_{\mathrm{O}_2}} \frac{\mathrm{d}^2 C_{\mathrm{O}_2}}{\mathrm{d}n^2} = -\frac{D_T}{2 L_{\mathrm{H_2O}}} \frac{\mathrm{d}^2 C_{\mathrm{H_2O}}}{\mathrm{d}n^2} = \frac{D_T}{2 L_{\mathrm{H}_2}} \frac{\mathrm{d}^2 C_{\mathrm{H}_2}}{\mathrm{d}n^2} = \omega_{4f}, \tag{18}$$

indicating that, in the first approximation, the fuel burns as dictated by the irreversible overall reaction $2H_2 + O_2 \rightarrow 2H_2O$ with a rate equal to that of reaction $4f$. At the same level of approximation, the energy conservation equation becomes

$$\rho c_p D_T \frac{\mathrm{d}^2 T}{\mathrm{d}n^2} = -2 q \omega_{4f}, \tag{19}$$

and diffusive transport of radicals can be neglected in (4)–(7) to give

$$\omega_1 - \omega_2 = 0 \tag{20}$$

$$\omega_1 + \omega_2 - \omega_3 + 2\omega_{5f} - \omega_{7f} = 0 \tag{21}$$

$$-\omega_1 + \omega_2 + \omega_3 - \omega_{4f} - \omega_{5f} - \omega_{6f} = 0 \tag{22}$$

$$\omega_{4f} - \omega_{5f} - \omega_{6f} - \omega_{7f} = 0. \tag{23}$$

In (19), $q = -h^o_{\mathrm{H_2O}}$ denotes the amount of heat released per mole of H_2 consumed. The new set of equations (18)–(23), including the steady-state approximations (20)–(23) for the

radicals, apply at leading order provided the radicals concentrations are much smaller than C_{H_2}.

Using the boundary conditions as $n \to \infty$ in integrating the first two equations in (18) yields

$$C_{O_2} = C_{O_{2b}} + \frac{L_{O_2}}{2L_{H_2}} C_{H_2} \tag{24}$$

$$C_{H_2O} = C_{H_2O_b} - \frac{L_{H_2O}}{L_{H_2}} C_{H_2} \tag{25}$$

while a similar integration of $d^2(\rho c_p T + q C_{H_2}/L_{H_2})/dn^2 = 0$, obtained from a linear combination of the last equation in (18) and (19), gives

$$T_b - T = q C_{H_2}/(\rho c_p L_{H_2}). \tag{26}$$

Equations (24)–(26) can be used to relate the concentrations of oxygen and water vapor and the temperature to the local H_2 concentration. In the computations below, the values $L_{O_2} = 1.11$, $L_{H_2} = 0.3$, $L_{H_2O} = 0.83$ are employed for the different Lewis numbers, and the constant values of the density and specific heat are evaluated at equilibrium.

To proceed with the analysis, (20)–(23) must be solved to give expressions for the radical concentrations [1]. If the reverse reaction $2b$ is neglected, an excellent approximation under these fuel-lean conditions, the resulting explicit expressions become

$$C_{O_{ss}} = \frac{\alpha k_{3f} C_{H_2}}{G k_{1b}} \left(\frac{k_{1f}}{\alpha k_{4f} C_M} - 1 \right) \tag{27}$$

$$C_{OH_{ss}} = \frac{k_{2f} C_{H_2}}{k_{1b}} \left(\frac{k_{1f}}{\alpha k_{4f} C_M} - 1 \right) \tag{28}$$

$$C_{H_{ss}} = \frac{1}{G} \frac{k_{2f} k_{3f} C_{H_2}^2}{k_{1b} k_{4f} C_M C_{O_2}} \left(\frac{k_{1f}}{\alpha k_{4f} C_M} - 1 \right), \tag{29}$$

$$C_{HO_{2ss}} = \frac{k_{3f}}{(f + G) k_{7f}} C_{H_2}, \tag{30}$$

where

$$f = \frac{k_{5f} + k_{6f}}{k_{7f}} \frac{k_{3f}}{k_{4f} C_M} \frac{C_{H_2}}{C_{O_2}}, \tag{31}$$

$$G = \frac{1 + \gamma_{3b}}{2} + \frac{f}{2} \left\{ [1 + 2(3 + \gamma_{3b})/f + (1 + \gamma_{3b})^2/f^2]^{1/2} - 1 \right\} \tag{32}$$

and

$$\alpha = \frac{k_{6f} f/(k_{5f} + k_{6f}) + G}{f + G}, \tag{33}$$

with

$$\gamma_{3b} = \frac{k_{3b} C_{H_2O}}{k_{4f} C_M C_{O_2}}. \tag{34}$$

Substituting the H-atom concentration (29) into the expression for ω_{4f} given in (15) provides an explicit non-Arrhenius expression for the overall rate of the global reaction $2H_2 + O_2 \rightarrow 2H_2O$.

It is of interest that, according to (27), (28) and (29), in the steady-state approximation adopted here the concentrations of O, OH and H vanish as the temperature approaches the crossover value T_c, defined by the condition

$$k_{1f} = \alpha k_{4f} C_M, \tag{35}$$

giving a value that depends on the composition through the function α and the effective third-body concentration C_M. At temperatures below T_c the steady-state approximation predicts $C_O = C_{OH} = C_H = 0$, while the concentration of the hydroperoxyl radical, given in (30), reaches a nonzero value at the crossover temperature and is positive also for $T < T_c$. In fact HO_2 continues to react for $T < T_c$ by steps not included in the seven-step mechanism; it is eventually consumed completely when $T = T_u$, but this chemistry exerts very small influences on burning rates, entirely negligible at the orders addressed here. Because of the linear dependence of ω_{4f} on the H-atom concentration, the overall oxidation reaction $2H_2 + O_2 \rightarrow 2H_2O$ is restricted to a high-temperature reaction layer adjacent to the flame hot boundary where the temperature lies in the range $T_c < T < T_b$. This layer is thin compared with the flame provided $T_b - T_c \ll T_b - T_u$, where the subscript u denotes unburnt conditions in the fresh mixture upstream from the deflagration. This requirement justifies the neglect of convective effects in the reaction layer.

Because of the relatively strong temperature sensitivity of the rate of the branching reaction $1f$, the cutoff factor $k_{1f}/(\alpha k_{4f} C_M) - 1$ readily takes on values of order unity across the thin reaction layer for relatively small values of the temperature increment $T_b - T_c$ of order $\beta_{1f}^{-1} T_c \ll T_b - T_u$,where $\beta_{1f} = T_{a_{1f}}/T_c + n_{1f} - n_{4f} + 1 \sim 10$ is an appropriately defined dimensionless activation temperature that accounts for the different algebraic temperature dependences present in $k_{1f}/(\alpha k_{4f} C_M)$. Under these conditions, Equation (29) indicates that

$$\frac{C_H}{C_{H_2}} \sim \frac{k_{2f} k_{3f}}{k_{1b} k_{1f}} \frac{k_{1f}}{k_{4f} C_M} \frac{C_{H_2}}{C_{O_2}}, \tag{36}$$

which can also be written in the form

$$\frac{C_H}{C_{H_2}} \sim \frac{k_{2f} k_{3f}}{k_{1b} k_{1f}} \frac{k_{1f}}{k_{4f} C_M} \frac{L_{H_2} C_{H_{2u}}}{C_{O_{2u}}} \frac{T_b - T_c}{T_b - T_u}, \tag{37}$$

where the value of the hydrogen–oxygen ratio C_{H_2}/C_{O_2} in the reaction zone has been evaluated approximately using (26) with $qC_{H_{2u}}/(\rho c_p) \simeq (T_b - T_u)$. Since the shuffle-reaction rate-constant factor $(k_{2f} k_{3f})/(k_{1b} k_{1f})$ is a quantity of order unity, e.g., $(k_{2f} k_{3f})/(k_{1b} k_{1f}) = 0.59$ at $T = 1000$ K, it is clear from (37) that the small value of $(T_b - T_c)/(T_b - T_u) \ll 1$ associated with the existence of a thin reaction layer is sufficient to guarantee the validity of the steady-state approximation for H atoms, which requires that $C_H/C_{H_2} \ll 1$

in the reaction zone. It is also of interest that, according to (27) and (28), for values of the cutoff factor $k_{1f}/(\alpha k_{4f} C_{\mathrm{M}}) - 1$ of order unity the O and OH concentrations satisfy $C_{\mathrm{O}}/C_{\mathrm{H_2}} \sim k_{3f}/k_{1b}$ and $C_{\mathrm{OH}}/C_{\mathrm{H_2}} \sim k_{2f}/k_{1b}$. The steady-state approximations for these two radicals are therefore directly related to the large value of k_{1b} relative to those of k_{3f} and k_{2f} (e.g., $k_{3f}/k_{1b} = 0.14$ and $k_{2f}/k_{1b} = 0.02$ at $T = 1000$ K), which causes the concentrations of O and OH to remain small compared to that of H_2. Similarly, with $f + G$ being typically of order unity, it follows from (30) that $C_{\mathrm{HO_2}}/C_{\mathrm{H_2}} \sim k_{3f}/k_{7f}$, again a very small quantity at the temperatures typically encountered in the reaction zone, e.g., $k_{3f}/k_{7f} = 0.04$ at $T = 1000$ K, thereby ensuring the accuracy of the HO_2 steady state.

Observation of (36) reveals that as the temperature difference $T_b - T_c$ increases, the ratio $C_{\mathrm{H}}/C_{\mathrm{H_2}}$ also increases, partly because of the dependence on $C_{\mathrm{H_2}}/C_{\mathrm{O_2}}$ and partly because of the exponential temperature dependence of $k_{1f}/(k_{4f} C_{\mathrm{M}})$, which would also enter through the cutoff factor appearing in (29), eventually leading to failure of the steady-state assumption for H atoms for sufficiently large values of $T_b - T_c$ such that $C_{\mathrm{H}} \sim C_{\mathrm{H_2}}$ in the reaction zone. Under these conditions, the one-step approximation must be replaced with a two-step description, as done in previous analyses of stoichiometric and moderately lean flames [7, 8]. It can be anticipated that, because of the temperature dependence of k_{1f}, the flame structure that replaces the steady-state regime analyzed here will show a relatively thin branching layer of radical production surrounded by thicker layers of radical recombination. The analysis of this multi-layer structure, not further considered here, should be addressed in future work.

To obtain the burning rate associated with the steady-state description the last equation in (18) multiplied by $\mathrm{d}C_{\mathrm{H_2}}/\mathrm{d}n$ may be integrated once with the boundary conditions as $n \to \pm\infty$ to give

$$(\dot{m}_{\mathrm{H_2}})_{ss} = 2W_{\mathrm{H_2}} \left(\frac{D_T}{L_{\mathrm{H_2}}} \int_0^{\infty} \omega_{4f} \mathrm{d}C_{\mathrm{H_2}} \right)^{1/2}. \tag{38}$$

Because of the reaction-rate cutoff at the crossover point, this expression becomes

$$(\dot{m}_{\mathrm{H_2}})_{ss} = 2W_{\mathrm{H_2}} \left(\frac{D_T}{L_{\mathrm{H_2}}} \int_0^{C_{\mathrm{H_2}c}} \frac{k_{2f} k_{3f} C_{\mathrm{H_2}}^2}{G k_{1b}} \left(\frac{k_{1f}}{\alpha k_{4f} C_{\mathrm{M}}} - 1 \right) \mathrm{d}C_{\mathrm{H_2}} \right)^{1/2}, \tag{39}$$

when the steady-state expression (29) is used to evaluate C_{H}. In the integration, use must be made of (26) to compute the temperature (and therefore evaluate the reaction-rate constants) in terms of $C_{\mathrm{H_2}}$. Similarly, the concentrations $C_{\mathrm{O_2}}$ and $C_{\mathrm{H_2O}}$, which enter in the computation of G, α and C_{M}, are to be evaluated from (24) and (25). The integration is extended until the H_2 concentration reaches its limiting value at crossover

$$C_{\mathrm{H_2}c} = \rho c_p L_{\mathrm{H_2}} (T_b - T_c)/q, \tag{40}$$

at which (35) is satisfied.

4. Sample leading-order results and useful simplifications

The burning rate given in (39) depends mainly on the burnt temperature T_b, which appears in (26), and on the pressure, which determines C_{M}, whereas the dependence on the burnt-gas composition through the values $C_{\mathrm{O_2}b}$ and $C_{\mathrm{H_2O}b}$ that enter in (24) and (25) is somewhat

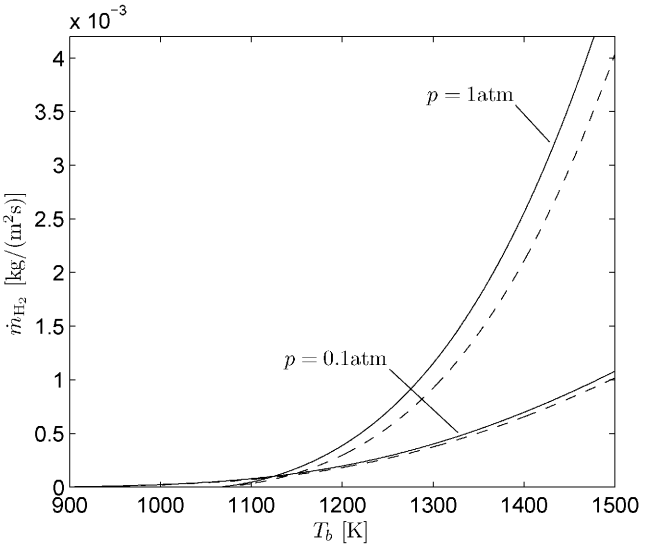

Figure 2. The variation with the burnt temperature T_b of the fuel burning rate $\dot{m}_{\mathrm{H}_2}$ for $p = 0.1$ atm and $p = 1$ atm as obtained from the evaluating the steady-state expression (39) (dashed curves) and from adding to this result the correction (73) due to steady-state failure in the crossover layer (solid curves); in the computation, for each T_b the values of $C_{\mathrm{O}_{2b}}$ and $C_{\mathrm{H}_2\mathrm{O}_b}$ are taken as the equilibrium values for a hydrogen–air planar deflagration with $T_u = 300$ K.

weaker, with the value of $C_{\mathrm{H}_2\mathrm{O}_b}$ affecting mainly the flammability limit, as discussed below. The variation of $(\dot{m}_{\mathrm{H}_2})_{ss}$ with the burnt temperature for $p = 0.1$ atm and $p = 1$ atm is shown in Figure 2. In the computation, for each value of T_b, the accompanying values of $C_{\mathrm{O}_{2b}}$ and $C_{\mathrm{H}_2\mathrm{O}_b}$ are selected as the downstream equilibrium values of a planar deflagration with $T_u = 300$ K and equivalence ratio ϕ such that the associated adiabatic flame temperature equals T_b. In the evaluation, the approximate expression $\rho D_T = 2.58 \times 10^{-5}(T/298)^{0.7}$ kg/(m s) [9] is used, and the NASA polynomial fits are employed in the evaluation of c_p.

The expression (39) predicts a burning rate $(\dot{m}_{\mathrm{H}_2})_{ss}$ that is positive provided the burnt temperature is sufficiently high for the cutoff factor $k_{1f}/(\alpha k_{4f} C_{\mathrm{M}}) - 1$ to be positive across the reactive layer. Correspondingly, the steady-state approximation provides a prediction for the lean flammability limit, associated with conditions such that the burnt temperature equals the critical crossover value $T_b = (T_c)_l$ below which $k_{1f}/(\alpha k_{4f} C_{\mathrm{M}}) - 1 < 0$ everywhere across the flame. As implied by (40), the hydrogen concentration in the reaction layer is very small near the flammability limit, so that in the first approximation one may take $\alpha = 1$ in (35) to compute the critical crossover value $(T_c)_l$ [1]. The resulting value depends through C_{M} on the pressure and also on the water vapor concentration $C_{\mathrm{H}_2\mathrm{O}_b}$, as can be seen in (16). When the equilibrium composition is computed as that of a planar deflagration, differences in $(T_c)_l$ appear for different values of T_u and of the initial composition. For instance, at $p = 1$ atm the resulting values are $(T_c)_l = (1072, 1064, 1054)$ K when $C_{\mathrm{H}_2\mathrm{O}_b} = (1.3, 1.15, 0.99)$ mol/m^3 is used in computing $k_{1f} = k_{4f} C_{\mathrm{M}}$, as corresponds to a planar H_2-air deflagration with $T_u = (200, 300, 400)$ K, while $(T_c)_l = (1075, 1067, 1057)$ for the values $C_{\mathrm{H}_2\mathrm{O}_b} = (1.35, 1.2, 1.04)$ mol/m^3 corresponding to a planar H_2-O_2 deflagration, also with $T_u = (200, 300, 400)$ K. These variations of the flammability limit can be readily incorporated when representing the temperature

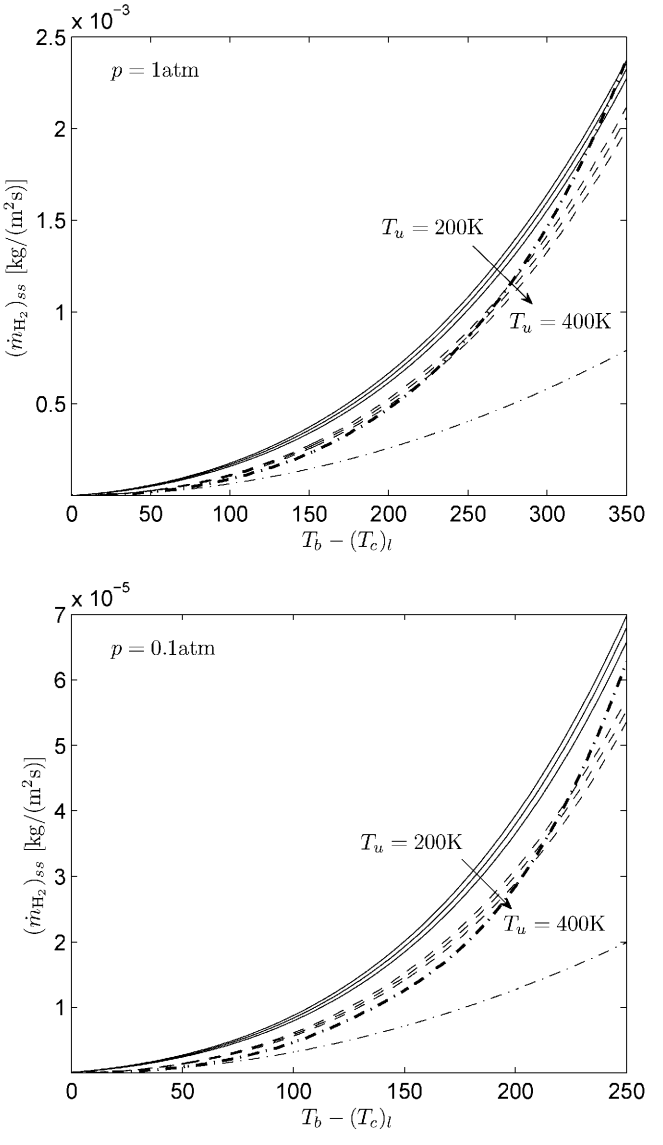

Figure 3. The variation with the temperature increment $T_b - (T_c)_l$ of the fuel burning rate $(\dot{m}_{\mathrm{H}_2})_{ss}$ of the steady-state region calculated from (39) for $p = 1$ atm (upper plot) and $p = 0.1$ atm (lower plot); in the computation, for each T_b the values of $C_{\mathrm{O}_{2b}}$ and $C_{\mathrm{H_2O}_b}$ are taken as the equilibrium values for a H_2-air (solid curves) and H_2-O_2 (dashed curves) planar deflagration with $T_u = (200, 300, 400)$ K. The dot-dashed lines correspond to results of evaluations of (42) (thin curve) and of (44) (thick curve) with the constant factor in square brackets evaluated with $G = 1$, $T = (T_c)_l$ and with the equilibrium composition at the flammability limit of a H_2-air deflagration with $T_u = 300$ K; they are essentially the same for H_2-air and H_2-O_2 systems.

variation of the burning rate by employing the temperature increment $T_b - (T_c)_l$. When this is done only relatively small differences in $(\dot{m}_{\mathrm{H}_2})_{ss}$ are found between the results obtained with different values of $C_{\mathrm{O}_{2b}}$ and $C_{\mathrm{H_2O}_b}$, as may be seen in Figure 3 for $p = 1$ atm and $p = 0.1$ atm.

Perturbations of (39) about the flammability conditions enable simplified expressions for $(\dot{m}_{\mathrm{H}_2})_{ss}$ in terms of $T_b - (T_c)_l$ to be derived. For instance, using

$$\frac{k_{1f}}{\alpha k_{4f} C_{\mathrm{M}}} - 1 \simeq \beta_{1f} \frac{T - (T_c)_l}{(T_c)_l}, \tag{41}$$

where $\beta_{1f} = T_{a_{1f}}/(T_c)_l + n_{1f} - n_{4f} + 1$ is the value of the dimensionless activation temperature introduced above (36) evaluated at the crossover temperature, and neglecting variations of all other reaction-rate constants along with departures of α from unity, it is found that (39) reduces to

$$(\dot{m}_{\mathrm{H}_2})_{ss} = 2W_{\mathrm{H}_2} \left[\frac{D_T}{12 L_{\mathrm{H}_2}} \frac{k_{2f} k_{3f}}{G k_{1b}} \left(\frac{\rho c_p L_{\mathrm{H}_2}}{q} \right)^3 \frac{\beta_{1f}}{(T_c)_l} \right]^{1/2} (T_b - (T_c)_l)^2, \tag{42}$$

where $G = 1 + \gamma_{3b}$ as corresponds to $C_{\mathrm{H}_2} = 0$. The factor in square brackets is to be evaluated at the flammability limit, yielding therefore a quadratic dependence of $(\dot{m}_{\mathrm{H}_2})_{ss}$ on the temperature increment $T_b - (T_c)_l$. Since γ_{3b} is typically small at the flammability limit, the approximate value $G \simeq 1$ can be assumed for simplicity in the evaluations, as done for the corresponding curves that are shown in Figure 3. As can be seen, the approximate solution (42) tends to underpredict the increase of $(\dot{m}_{\mathrm{H}_2})_{ss}$ with $T_b - (T_c)_l$, although it becomes a reasonable approximation as the flammability limit is approached. Better agreement away from the limit is obtained when the exponential temperature variation of the different reaction-rate constants is retained by expressing (39) in terms of the dimensionless rescaled temperature increments

$$\theta = \beta_{1f} \frac{T - (T_c)_l}{(T_c)_l} \quad \text{and} \quad \theta_b = \beta_{1f} \frac{T_b - (T_c)_l}{(T_c)_l} \tag{43}$$

with (26) used to relate the variations of C_{H_2} and temperature, yielding

$$(\dot{m}_{\mathrm{H}_2})_{ss} = 2W_{\mathrm{H}_2} \left[\frac{D_T}{L_{\mathrm{H}_2}} \frac{k_{2f} k_{3f}}{G k_{1b}} \left(\frac{\rho c_p L_{\mathrm{H}_2}}{q} \right)^3 \left(\frac{(T_c)_l}{\beta_{1f}} \right)^3 \right]^{1/2} \times [H(\theta_b)]^{1/2}. \tag{44}$$

The integral

$$H(\theta_b) = \int_0^{\theta_b} e^{\beta\theta} (e^{\theta} - 1)(\theta_b - \theta)^2 \mathrm{d}\theta \tag{45}$$

can be integrated explicitly to give

$$\begin{aligned} H(\theta_b) = {} & 2e^{\beta\theta_b} \left(\frac{e^{\theta_b}}{(\beta+1)^3} - \frac{1}{\beta^3} \right) \\ & + \frac{\theta_b^2}{\beta(\beta+1)} + \frac{2\theta_b(1+2\beta)}{\beta^2(\beta+1)^2} + \frac{2(3\beta^2+3\beta+1)}{\beta^3(\beta+1)^3} \end{aligned} \tag{46}$$

which takes on the limiting values $H = 2\exp[(\beta+1)\theta_b]/(\beta+1)^3$ for $\theta_b \gg 1$ and $H = \theta_b^4/12$ for $\theta_b \ll 1$, the latter limit indicating that (44) reduces naturally to (42) as the flammability limit is approached. Note that the temperature variation of the factor $k_{2f}k_{3f}/k_{1b}$ enters in (45) through the term $e^{\beta\theta}$, where $\beta = [(T_{a_{2f}} + T_{a_{3f}} - T_{a_{1b}})/(T_c)_l + n_{2f} + n_{3f} - n_{1b} - 2]/\beta_{1f}$. The expression (44) is seen to approximate reasonably well the burning rate (39), as can be seen in Figure 3, which shows results for two different pressures.

The approximate burning-rate laws (42) and (44) can be useful for theoretical analysis of flame stability near the lean flammability limit. In particular, these expressions predict an effective activation energy that becomes singular according to

$$\frac{T_b}{(\dot{m}_{\mathrm{H_2}})_{ss}}\frac{\mathrm{d}(\dot{m}_{\mathrm{H_2}})_{ss}}{\mathrm{d}T_b} = \frac{2T_b}{T_b - (T_c)_l} \tag{47}$$

as the flammability limit is approached, i.e., as $T_b \to (T_c)_l$, thereby promoting flame instability.

Although the burning-rate results that have been discussed here provide reasonable accuracy for most purposes, there is interest in seeking better accuracy. Before considering other aspects of the reaction-layer structure that can significantly improve accuracies of burning-rate predictions, it is worth commenting further on the determination of the kinetically controlled flammability limit arising with the seven elementary reactions of Table 1. We have used above the equation $k_{1f} = k_{4f}C_{\mathrm{M}}$ to determine the critical temperature $(T_c)_l$, and assume that no flame may exist when the burnt temperature T_b lies below that temperature. For a hydrogen–air mixture with $p = 1$ atm and $T_u = 300$ K, this simple criterion gives $(T_c)_l = 1064$ K and $\phi_l = 0.251$. The numerical computations with the COSILAB code for the seven-step mechanism yield however a small but finite flame propagation velocity $v_l \simeq 2$ mm/s at these conditions, and they also predict flames to exist for equivalence ratios in the range $0.249 \lesssim \phi < 0.251$. This very small difference is associated with complexities that arise from the steady-state approximation very near the flammability limit and that increase in importance with decreasing pressure but still produce only small effects. The complexity is related to the variation of α near the hot boundary under conditions close to the flammability limit.

Normally the cutoff factor $k_{1f}/(\alpha k_{4f}C_{\mathrm{M}}) - 1$ in (39) increases monotonically with temperature because of the increase of k_{1f}. For conditions near the flammability limit, however, very near the hot boundary it is found that the factor α increases with temperature more rapidly, causing the cutoff factor to decrease with temperature. This occurs because of the decrease of f with decreasing $C_{\mathrm{H_2}}$, according to (31), which is seen from (33) to produce an increase in α. Under conditions that are extremely close to the flammability limit this effect in fact causes the cutoff factor to reach zero again just upstream from the hot boundary, leading to fuel leakage according to the steady-state approximations that have been employed over an extremely small range of conditions near the flammability limit. This effect increases with decreasing pressure and with increasing dilution, as may be inferred from (31), and it does not occur for H_2-O_2 systems at the pressures for which results are shown below.

A more formal analysis, to be formulated in the following section as an asymptotic expansion in the small parameter ε of Equation (52), shows that as the downstream boundary is approached and the cutoff factor as well as the properly scaled radical concentrations y_{O}, y_{OH} and y_{H} become of order ε, the steady-state approximation must be replaced by a diffusion-reaction balance. This will be evident from Equation (64) in the following section. Although there is a consequent correction to the burning rate, this correction is of order ε

and therefore is small compared with the correction to be derived in the following section. Even when the cutoff factor does not become small at the hot boundary, a diffusive-reactive character arises where y_O and y_{OH} decrease to order ε, but under conditions very near the limit, when this factor does become sufficiently small, there may well be fuel leakage that results in a downstream convective-reactive zone not described by the starting equations of the present paper. Since these intricacies affect neither burning rates nor flammability limits significantly, they are not addressed in the present paper.

5. The crossover layer

The accuracy of the explicit steady-state expression (29) is demonstrated in the inset of Figure 1, which includes the comparison of the H-atom profile determined numerically on the basis of the seven-step mechanism with that determined from evaluating (29). In the evaluation, use has been made of the profiles of reactant and water-vapor mol fractions and of temperature obtained numerically with the seven-step mechanism. It can be seen that the accuracy of the steady-state expression is excellent across the reaction layer, except at crossover, where the steady state predicts H atoms to disappear abruptly, thereby giving a profile with a discontinuous slope. Diffusive transport enters to remove this discontinuity, so that a smooth corner-layer profile replaces the abrupt change of the steady-state prediction when the seven-step mechanism is employed in the computations. Because of the direct proportionality of the burning rate and the H-atom content displayed in (17), the increased H-atom concentration in the layer of steady-state failure provides a nonnegligible additional contribution to the burning rate, which needs to be computed for increased accuracy.

Failure of the steady states for the radicals O, OH and H at a given upstream location is somewhat unexpected. To better clarify the problem it is of interest to write the radical conservation equations in dimensionless form, an effort that serves to identify the small parameter underlying the validity of the steady-state assumptions and the magnitude of the errors expected from the present analytical development. For that purpose, the fuel concentration is scaled with its crossover value $C_{H_{2c}}$ according to $y_{H_2} = C_{H_2}/C_{H_{2c}}$, whereas the radical concentrations $y_O = C_O/C_{O_o}$, $y_{OH} = C_{OH}/C_{OH_o}$ and $y_H = C_H/C_{H_o}$ are scaled with their characteristic values implied by (27)–(29)

$$C_{O_o} = \alpha \frac{k_{3f} C_{H_{2c}}}{G k_{1b}} \tag{48}$$

$$C_{OH_o} = \frac{k_{2f} C_{H_{2c}}}{k_{1b}} \tag{49}$$

$$C_{H_o} = \frac{1}{G} \frac{k_{2f} k_{3f} C_{H_{2c}}^2}{k_{1b} k_{4f} C_M C_{O_{2c}}}, \tag{50}$$

where the different reaction-rate constants are evaluated at the crossover temperature, which is also used in evaluating the effective third-body concentration C_M and the functions f and G from (16), (31), and (32), respectively, with the oxygen and water vapor concentrations evaluated from (24) and (25) with the H_2 concentration reached at crossover, that is from (40).

The characteristic thickness of the reaction region

$$\delta = [D_T/(k_{4f} C_M C_{O_{2c}} \varepsilon)]^{1/2}, \tag{51}$$

arising from an order-of-magnitude analysis of the last equation in (18), is employed to scale the dimensionless coordinate $x = n/\delta$, with

$$\varepsilon = \frac{C_{\mathrm{H}_o}}{C_{\mathrm{H}_{2_c}}} = \frac{1}{G}\frac{k_{2f}k_{3f}C_{\mathrm{H}_{2_c}}}{k_{1b}k_{4f}C_{\mathrm{M}}C_{\mathrm{O}_{2_c}}} \tag{52}$$

representing the characteristic H-to-H_2 concentration ratio, the small parameter for our steady-state analysis. Introducing these variables reduces (4)–(6) to the dimensionless form

$$-\varepsilon\frac{\Lambda_{\mathrm{O}}}{L_{\mathrm{O}}}\frac{\mathrm{d}^2 y_{\mathrm{O}}}{\mathrm{d}x^2} = \frac{k_{1f}}{k_{4f}C_{\mathrm{M}}}y_{\mathrm{H}} - \alpha(y_{\mathrm{OH}}y_{\mathrm{O}} + y_{\mathrm{H}_2}y_{\mathrm{O}}) \tag{53}$$

$$-\varepsilon\frac{\Lambda_{\mathrm{OH}}}{L_{\mathrm{OH}}}\frac{\mathrm{d}^2 y_{\mathrm{OH}}}{\mathrm{d}x^2} = \frac{k_{1f}}{k_{4f}C_{\mathrm{M}}}y_{\mathrm{H}} - \alpha(y_{\mathrm{OH}}y_{\mathrm{O}} - y_{\mathrm{H}_2}y_{\mathrm{O}}) - (2+\gamma_{3b})(y_{\mathrm{H}_2}y_{\mathrm{OH}} - y_{\mathrm{H}}) - 2\alpha y_{\mathrm{H}} \tag{54}$$

$$-\varepsilon\frac{1}{L_{\mathrm{H}}}\frac{\mathrm{d}^2 y_{\mathrm{H}}}{\mathrm{d}x^2} = -\frac{k_{1f}}{k_{4f}C_{\mathrm{M}}}y_{\mathrm{H}} + \alpha(y_{\mathrm{OH}}y_{\mathrm{O}} + y_{\mathrm{H}_2}y_{\mathrm{O}}) + (2+\gamma_{3b})(y_{\mathrm{H}_2}y_{\mathrm{OH}} - y_{\mathrm{H}}) \tag{55}$$

where we have neglected the reverse of reaction 2, along with the variation of C_{O_2} and $C_{\mathrm{H}_2\mathrm{O}}$ from their crossover values $C_{\mathrm{O}_{2_c}}$ and $C_{\mathrm{H}_2\mathrm{O}_c}$ and the temperature dependence of the different reaction-rate constants, except that of reaction $1f$, whose sensitivity near crossover must be taken into account. To achieve a more compact form, we have used the steady-state Equation (7) to write $-\omega_{5f} - \omega_{6f} = -\omega_{4f} + \omega_{7f}$ in (6), and neglect the H_2 variation when writing ω_{5f} in (5). The constant radical-radical ratios $\Lambda_{\mathrm{O}} = C_{\mathrm{O}_o}/C_{\mathrm{H}_o}$ and $\Lambda_{\mathrm{OH}} = C_{\mathrm{OH}_o}/C_{\mathrm{H}_o}$ appear as factors of order unity. Since the hydroperoxyl steady-state approximation does not fail, one may use in the first approximation

$$C_{\mathrm{HO}_2} = \frac{k_{3f}}{(f+G)k_{7f}}C_{\mathrm{H}_{2_c}}y_{\mathrm{H}_2} \tag{56}$$

for the present purposes. The radical Lewis numbers $L_{\mathrm{H}} = 0.18$, $L_{\mathrm{O}} = 0.7$ and $L_{\mathrm{OH}} = 0.73$ are used below in the numerical evaluations.

Equations (53)–(55) are the dimensionless form of (4)–(6). Although they are simplified by evaluating at crossover the O_2 and H_2O concentrations as well as all of the reaction-rate constants but k_{1f}, they still retain the essential nonlinearities of the problem, associated with consumption of fuel and with the temperature variation of the chain-branching controlling reaction $1f$. One could in principle write similar conservation equations for y_{H_2} and T/T_c to provide the dimensionless formulation of the burning-rate problem, to be solved by appropriately matching expansions of the different variables in powers of the asymptotically small parameter ε, but these additional equations are unnecessary for computing the H-atom concentration near crossover and are therefore omitted here.

Observation of (53)–(55) reveals that radical diffusion is negligible at leading order when the H-to-H_2 characteristic ratio ε is small, and the steady-state expressions

$$y_{\mathrm{O}_{ss}} = y_{\mathrm{OH}_{ss}} = y_{\mathrm{H}_{ss}}/y_{\mathrm{H}_2} = \left(\frac{k_{1f}}{\alpha k_{4f}C_{\mathrm{M}}} - 1\right)y_{\mathrm{H}_2} \tag{57}$$

are recovered, as corresponds to the dimensionless form of (27)–(29) under the simplifying assumptions listed before Equation (56). These expressions apply, with relative errors of

order ε, for $x > 0$, with the arbitrary origin of x assumed to be at the crossover point, where $k_{1f} = \alpha k_{4f} C_{\mathrm{M}}$, whereas $y_{\mathrm{O}} = y_{\mathrm{OH}} = y_{\mathrm{H}} = 0$ for $x < 0$. The steady-state approximations therefore hold provided $\varepsilon \ll 1$, so that evaluation of (52) serves to test the validity of the above development leading to (27)–(30). Note also that the steady-state description in the region $x \sim O(1)$ can be in principle improved by introducing expansions for the different dimensionless radical concentrations in ascending powers of ε. The analysis is not further pursued here because the associated relative corrections to the burning rate $(\dot{m}_{\mathrm{H}_2})_{ss}$ would be of order ε, smaller than the corrections, of order $\varepsilon^{2/3}$, arising from failure of the steady-state assumption at crossover, to be investigated below.

Due to their discontinuous gradients, the steady-state radical profiles do not constitute an acceptable solution at $x = 0$, because they would be associated with infinite values of the diffusive rates appearing on the left-hand sides of (53)–(55). In the solution that appears, radical diffusion becomes comparable to the chemical rates, yielding smooth profiles centered around $x = 0$ for the radicals, as seen for H in the seven-step computation shown in Figure 1. Failure of the steady-state approximation occurs at distances $x \sim \varepsilon^{1/3}$, where $y_{\mathrm{O}} \sim y_{\mathrm{OH}} \sim y_{\mathrm{H}} \sim 1 - y_{\mathrm{H}_2} \sim \varepsilon^{1/3}$ and $k_{1f}/(\alpha k_{4f} C_{\mathrm{M}}) = 1 + Ax$, where

$$A = \frac{\mathrm{d}}{\mathrm{d}x}\left(\frac{k_{1f}}{\alpha k_{4f} C_{\mathrm{M}}}\right) = \delta \frac{T_{1f}}{T_c^2}\left(\frac{\mathrm{d}T}{\mathrm{d}n}\right)_c , \tag{58}$$

as implied by a Taylor expansion near $x = 0$ with account taken of the temperature sensitivity of k_{1f}. The resulting factor A is of order $T_{1f}(T_b - T_c)/T_c^2$. Note that the temperature gradient in (58) can be related to the burning rate of the steady-state region through (9), giving

$$\left(\frac{\mathrm{d}T}{\mathrm{d}n}\right)_c = \frac{q}{\rho c_p}\frac{(\dot{m}_{\mathrm{H}_2})_{ss}}{W_{\mathrm{H}_2} D_T}. \tag{59}$$

Introducing into (53)–(55) expansions for the radicals of the form $y_{\mathrm{O}} = \varepsilon^{1/3}(\varphi_{\mathrm{O}}^0 + \varepsilon^{1/3}\varphi_{\mathrm{O}}^1 \cdots)$, $y_{\mathrm{OH}} = \varepsilon^{1/3}(\varphi_{\mathrm{OH}}^0 + \varepsilon^{1/3}\varphi_{\mathrm{OH}}^1 \cdots)$, and $y_{\mathrm{H}} = \varepsilon^{1/3}(\varphi_{\mathrm{H}}^0 + \varepsilon^{1/3}\varphi_{\mathrm{H}}^1 \cdots)$ yields at leading order the linear homogeneous problem

$$0 = \alpha(\varphi_{\mathrm{H}}^0 - \varphi_{\mathrm{O}}^0) \tag{60}$$

$$0 = -\alpha(\varphi_{\mathrm{H}}^0 - \varphi_{\mathrm{O}}^0) - (2 + \gamma_{3b})(\varphi_{\mathrm{OH}}^0 - \varphi_{\mathrm{H}}^0) \tag{61}$$

$$0 = -\alpha(\varphi_{\mathrm{H}}^0 - \varphi_{\mathrm{O}}^0) + (2 + \gamma_{3b})(\varphi_{\mathrm{OH}}^0 - \varphi_{\mathrm{H}}^0). \tag{62}$$

This problem has a nontrivial solution with

$$\varphi_{\mathrm{O}}^0 = \varphi_{\mathrm{OH}}^0 = \varphi_{\mathrm{H}}^0 \tag{63}$$

because the determinant of the coefficient matrix is zero, as can be seen by noticing that the sum 2 × (60) + (61) + (62) is identically zero. The solution can be found by writing the accompanying linear combination 2 × (53) + (54) + (55) of the radical conservation equations, leading to

$$-\frac{\varepsilon}{2\alpha}\frac{\mathrm{d}^2}{\mathrm{d}x^2}\left(\frac{2\Lambda_{\mathrm{O}}}{L_{\mathrm{O}}} y_{\mathrm{O}} + \frac{\Lambda_{\mathrm{OH}}}{L_{\mathrm{OH}}} y_{\mathrm{OH}} + \frac{1}{L_{\mathrm{H}}} y_{\mathrm{H}}\right) = \left(\frac{k_{1f}}{\alpha k_{4f} C_{\mathrm{M}}} - 1\right) y_{\mathrm{H}} - y_{\mathrm{OH}} y_{\mathrm{O}}. \tag{64}$$

From this result it is seen that near crossover the evolution of the radical pool depends on the balance between radical loss by diffusion (the terms on the left-hand side), radical production (the first term on the right-hand side), arising from departures from the crossover temperature, and radical consumption through reaction $1b$ (the second term on the right-hand side). Introducing the expansions for y_i together with (63) provides the reduced problem

$$\frac{\mathrm{d}^2\varphi}{\mathrm{d}\xi^2} = \varphi(\varphi - \xi), \quad \varphi(-\infty) = \varphi(+\infty) - \xi = 0, \tag{65}$$

where the radical pool concentration

$$\varphi = \frac{\varphi_{\mathrm{H}}^0}{[BA^2/(2\alpha)]^{1/3}} \tag{66}$$

has been introduced, along with the rescaled coordinate

$$\xi = \frac{x}{[B\varepsilon/(2\alpha A)]^{1/3}}, \tag{67}$$

where

$$B = \frac{2\Lambda_{\mathrm{O}}}{L_{\mathrm{O}}} + \frac{\Lambda_{\mathrm{OH}}}{L_{\mathrm{OH}}} + \frac{1}{L_{\mathrm{H}}}. \tag{68}$$

The problem defined by (65) was first encountered by Liñán in analyzing the inner structure of diffusion flames for large Damkohler numbers [10]. It is equivalent to a problem often attributed to Friedlander and Keller [11] whose solution in the combustion context was

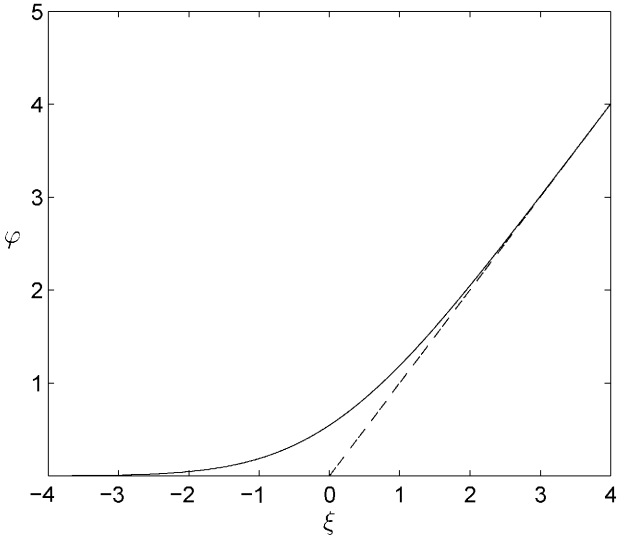

Figure 4. The rescaled radical concentration in the crossover layer as determined from numerical integration of (65); the dashed line represents the asymptote $\varphi = \xi$ corresponding to $\xi \to \infty$.

first published by Fendell [12]; see Williams [13]. The resulting solution is plotted for completeness in Figure 4.

According to (17), the departures of the H-atom concentration from its steady-state value (29) result in corrections to the burning rate

$$\dot{m}_{\mathrm{H}_2} - (\dot{m}_{\mathrm{H}_2})_{ss} = 2W_{\mathrm{H}_2} \int_{-\infty}^{+\infty} k_{4f} C_{\mathrm{M}} C_{\mathrm{O}_2} (C_{\mathrm{H}} - C_{\mathrm{H}_{ss}}) \mathrm{d}n, \tag{69}$$

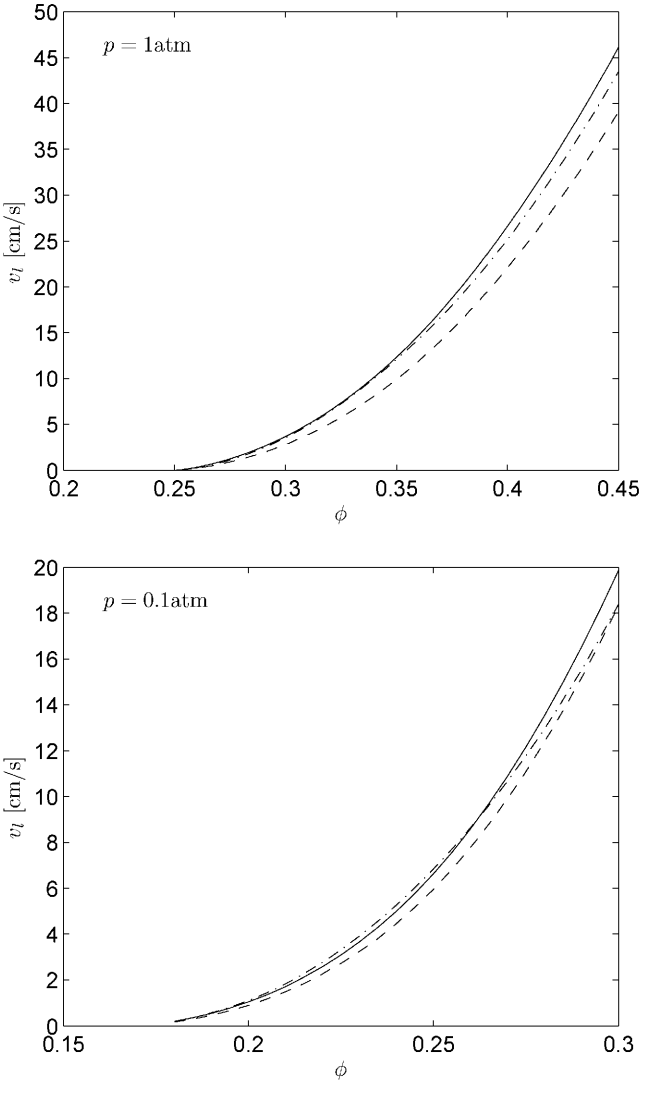

Figure 5. The variation with equivalence ratio of the planar propagation velocity of a premixed hydrogen–air flame for $p = 1$ atm (upper plot) and $p = 0.1$ atm (lower plot) as obtained for $T_u = 300$ K from the steady-state burning-rate prediction $v_l = \dot{m}_{\mathrm{H}_2}/(W_{\mathrm{H}_2} C_{\mathrm{H}_{2u}})$ (dashed curves), from the burning-rate prediction including the contribution of the crossover layer $v_l = \dot{m}_{\mathrm{H}_2}/(W_{\mathrm{H}_2} C_{\mathrm{H}_{2u}})$ (solid curves), and from numerical integrations with the seven-step short mechanism listed in Table 1 (dot-dashed curves).

which can be alternatively written in the simplified form

$$\dot{m}_{\mathrm{H}_2} - (\dot{m}_{\mathrm{H}_2})_{ss} = 2W_{\mathrm{H}_2} C_{\mathrm{H}_o} \delta \int_{-\infty}^{+\infty} k_{4f} C_{\mathrm{M}} C_{\mathrm{O}_2} (y_{\mathrm{H}} - y_{\mathrm{H}_{ss}}) \mathrm{d}x. \tag{70}$$

Regarding this last equation it is clear that the errors of the steady-state approximation in the region $x \sim O(1)$, where $y_{\mathrm{H}} - y_{\mathrm{H}_{ss}} \sim \varepsilon$, produces small relative errors $(\dot{m}_{\mathrm{H}_2} - \dot{m}_{\mathrm{H}_{2ss}})/\dot{m}_{\mathrm{H}_2} \sim \varepsilon$, whereas the departures $y_{\mathrm{H}} - y_{\mathrm{H}_{ss}} \sim \varepsilon^{1/3}$ seen in the crossover layer $x \sim \varepsilon^{1/3}$ gives a much larger contribution to the burning rate, of order $(\dot{m}_{\mathrm{H}_2} - \dot{m}_{\mathrm{H}_{2ss}})/\dot{m}_{\mathrm{H}_2} \sim \varepsilon^{2/3}$. This last correction can be evaluated explicitly by introducing in (70) the inner variables φ and ξ to give

$$\dot{m}_{\mathrm{H}_2} - (\dot{m}_{\mathrm{H}_2})_{ss} = 2I W_{\mathrm{H}_2} (k_{4f} C_{\mathrm{M}} C_{\mathrm{O}_2})_c C_{\mathrm{H}_o} \delta \varepsilon^{2/3} \left(\frac{B}{2\alpha} \right)_c^{2/3} A^{1/3}, \tag{71}$$

where the integral factor

$$I = \int_{-\infty}^{0} \varphi \mathrm{d}\xi + \int_{0}^{\infty} (\varphi - \xi) \mathrm{d}\xi = 0.95. \tag{72}$$

accounts for the increase in radical concentration from the steady-state prediction. Substitutions from (48)–(52), (58), (59) and (68) enable (71) to be written explicitly as

$$\begin{aligned} \dot{m}_{\mathrm{H}_2} - (\dot{m}_{\mathrm{H}_2})_{ss} = 2I & \left(\frac{k_{3f}}{G k_{1b}} \right)_c [D_T W_{\mathrm{H}_2}^2 k_{2f} C_{\mathrm{H}_{2e}}^3 (\dot{m}_{\mathrm{H}_2})_{ss}]_c^{1/3} \left(\frac{q C_{\mathrm{H}_{2e}} T_{1f}}{\rho c_p T_c^2} \right)^{1/3} \\ & \times \left(\frac{1}{L_{\mathrm{O}}} + \frac{G k_{2f}}{2\alpha k_{3f} L_{\mathrm{OH}}} + \frac{k_{2f} C_{\mathrm{H}_{2e}}}{2\alpha k_{4f} C_{\mathrm{M}} C_{\mathrm{O}_2} L_{\mathrm{H}}} \right)_c^{2/3}, \end{aligned} \tag{73}$$

where α and G can be determined from (31)–(34).

The corrected burning rate, including the increase (73) due to the additional contribution of the crossover layer, is plotted in Figure 2 for $p = 1$ atm and $p = 0.1$ atm. The extent of the resulting correction is tested in Figure 5, which compares laminar flame propagation velocities obtained from seven-step chemistry with the burning-rate predictions $v_l = \dot{m}_{\mathrm{H}_2}/(W_{\mathrm{H}_2} C_{\mathrm{H}_{2u}})$. As can be seen, incorporating the correction due to steady-state failure improves considerably the prediction of v_l near the flammability limit, its effect being quantitatively more significant at atmospheric conditions.

6. Conclusions and future work

Near the lean flammability limit hydrogen–air and hydrogen–oxygen flames exhibit an extended preheat zone followed by a reaction zone, the structure of which is analyzed here as an asymptotic expansion in a small parameter ε representing the order of magnitude of the ratio of the H-atom concentration to the H_2 concentration in that zone. The analysis demonstrated that throughout most of the reaction zone the reaction intermediates closely maintain chemical-kinetic steady states, resulting in a one-step approximation for the combustion chemistry. In this approximation the reaction rate is zero below a cutoff temperature at which the rate of the branching step $H + O_2 \rightarrow OH + O$ equals the rate of the termination step $H + O_2 + M \rightarrow HO_2 + M$ for this chain reaction. The resulting non-Arrhenius rate

formula was employed to derive an expression for the burning rate in terms of an integral that can be evaluated numerically, and the lean flammability limit was obtained as the condition that this burning rate is zero, a kinetically controlled limit associated with the burnt-gas temperature becoming equal to a crossover temperature at which the branching and termination rates become equal. Simplified explicit formulas for the burning rate also were derived which produce values of burning rates that agree reasonably well with burning rates calculated by evaluating the integral numerically or by employing detailed chemistry. It was found, in particular, that similar to earlier results [8], as the lean flammability limit is approached, the burning rate becomes proportional to the square of the difference between the adiabatic flame temperature and the crossover temperature, leading to an effective overall activation temperature of four times the square of the flame temperature divided by this temperature difference, thus approaching infinity at the lean limit.

The steady-state approximation was found to fail in a region where the temperature is near the crossover temperature, having thickness of order $\varepsilon^{1/3}$ times the total reaction-zone thickness. The approximation also fails near the hot boundary. In these failure regions a one-step approximation to the chemistry no longer exists. Burning-rate corrections associated with failure near the hot boundary are of order ε and turn out to be negligible. However, those associated with failure near crossover, of order $\varepsilon^{2/3}$, are more significant. Analysis of the layer near crossover revealed its character to be that of a corner layer, the structure of which can be expressed in terms of a universal solution previously obtained for diffusion flames at large Damköhler numbers. Use of this solution provides an explicit correction to the burning rate that improves agreement with results obtained from numerical integrations with detailed chemistry, especially near normal atmospheric pressure. Above atmospheric pressure, HO_2 increasingly contributes to the burning rate, so that the chemistry on which the present analysis is based becomes increasingly inaccurate.

Future research could extend this type of analysis to higher pressures, addressing more complex chemistry. The results that have been obtained here can, however, be employed directly to study deflagration problems of interest at normal atmospheric pressure, or at somewhat reduced pressures. It is well known that lean hydrogen flames exhibit strong diffusive-thermal instabilities [14], and nonplanar models for deflagration structures under such conditions have been investigated [15]. Burning-rate and flammability-limit descriptions are needed for analyzing the stability and dynamics of the deflagrations that occur in these lean mixtures. The studies must take into account effects of curvature and strain. The forms of the results developed here can be readily employed in such studies, enabling the future investigations to focus on the transport and flow aspects of the problem, with the chemistry restricted to the interiors of surfaces whose properties have been obtained here. The present results can be employed directly in this future work, whether it is analytical or computational, so long as gradients downstream from the reaction zones investigated here are not steep enough to affect their structures.

For instance, effects of strain could be addressed by consideration of premixed flames in a counterflow configuration in which a fresh mixture flows against a nonreacting stream or a stream of combustion products. For weak values of the strain rate smaller than the reciprocal of the residence time across the flame, the flame lies on the fresh side outside the mixing layer, so that the structure of the reaction layer becomes independent of the product-side temperature. In obtaining the solution, the reaction zone could be treated as a discontinuity, with vanishing downstream gradients and with upstream gradients towards the fresh side given in (9) in terms of the burning rate. In this case, the burning-rate computations presented above could be employed directly to close the problem. Note that for these weakly strained flames, differential diffusion of hydrogen enters in the preheat

region, resulting in a value of the burnt temperature above the adiabatic flame temperature of the fresh mixture. As a result, stretched flames may be anticipated to exist for equivalence ratios below the kinetically controlled lean flammability limit of freely propagating planar flames. As the strain rate increases, the reaction zone moves into the mixing layer; in nonadiabatic configurations with reduced product-side temperatures, downstream heat loss from the reaction zone may then become important, reducing the burnt temperature, which may approach the crossover value, thereby leading to strain-induced extinction.

Future investigations of the type outlined above for stretched flames, as well as investigations of curved flames, can therefore benefit from the present results. The associated research efforts would be relevant to safety issues associated with increased utilization of hydrogen as well as to the operation and performance of devices that employ the combustion of hydrogen.

References

[1] D. Fernández-Galisteo, A.L. Sánchez, A. Liñán, and F.A. Williams, *One-step reduced kinetics for lean hydrogen–air deflagration*, Combust. Flame 156 (2009), pp. 985–996.

[2] Available at: http://maemail.ucsd.edu/combustion/cermech.

[3] P. Saxena and F.A. Williams, *Testing a small detailed chemical-kinetic mechanism for the combustion of hydrogen and carbon monoxide*, Combust. Flame 145 (2006), pp. 316–323.

[4] Cosilab Collection, Version 2.0.7, Rotexo-Softpredict-Cosilab GmbH & Co. KG, Bad Zwischenahn (Germany), www.SoftPredict.com (2007).

[5] J. Troe, *Detailed modeling of the temperature and pressure dependence of the reaction* $H+O_2+(M) \rightarrow HO_2+(M)$, Proc. Combust. Inst. 28 (2000), pp. 1463–1469.

[6] J.F. Grcar, *A new type of steady and stable, laminar, premixed flame in ultra-lean, hydrogen–air combustion*, Proc. Combust. Inst. 32 (2009), pp. 1011–1018.

[7] F. Mauss, N. Peters, B. Rogg, and F.A. Williams, *Reduced kinetic mechanisms for premixed hydrogen flames*, in *Reduced Kinetic Mechanisms for Applications in Combustion Systems*, N. Peters, B. Rogg, eds., Springer-Verlag, Heidelberg, 1993, pp. 29–43.

[8] K. Seshadri, N. Peters and F.A. Williams, *Asymptotic analysis of stoichiometric and lean hydrogen–air flames*, Combust. Flame 96 (1994), pp. 407–427.

[9] M.D. Smooke, and V. Giovangigli, *Formulation of the premixed and non-premixed test problems*, in *Mechanisms and Asymptotic Approximations for Methane–Air Flames* (Lecture Notes in Physics, Vol. 384), M.D. Smooke, ed., Springer-Verlag, Berlin, 1991, pp. 1–28.

[10] A. Liñán, *On the internal structure of laminar diffusion flames*, OSR/EOAR, TN 62–69, INTA, Madrid (1961).

[11] S.K. Friedlander and K.H. Keller, *The structure of the zone of diffusion controlled reaction*, Chem. Eng. Sci. 18 (1963), pp. 365–375.

[12] F.E. Fendell, *Ignition and extinction in combustion of initially unmixed reactants*, J. Fluid Mech. 21 (1965), pp. 281–303.

[13] F.A. Williams, *Theory of combustion in laminar flows*, Ann. Rev. Fluid Mech. 3 (1971), pp. 172–174.

[14] H.F. Coward and F. Brinsley, *The dilution limits of inflammability of gaseous mixtures*, J. Chem. Soc. 105 (1914), pp. 1859–1866.

[15] F.A. Williams and J.F. Grcar, *A hypothetical burning-velocity formula for very lean hydrogen–air mixtures*, Proc. Combust. Inst. 32 (2009), pp. 1351–1357.